Experimental study of multiple-intermittent cryogen spurts and laser pulses for the treatment of port wine stain birthmarks

Guillermo Aguilar[1,2], Bernard Choi[1], John A. Viator[1], Dan Andersen[3], and J. Stuart Nelson[1,2]

[1]Beckman Laser Institute, University of California, Irvine, CA 92612
[2]Department of Biomedical Engineering, University of California, Irvine, CA 92612
[3]Lumenis Inc., 2400 Condensa St., Santa Clara, CA 95051

ABSTRACT

Cryogen spray cooling (CSC) is used to minimize the risk of epidermal damage during pulsed laser treatment of port wine stain (PWS) birthmarks. Unfortunately, the current approach to CSC does not provide the necessary epidermal protection for all patients, particularly those with darker skin types. Therefore, alternative approaches need to be sought to improve PWS laser therapy.

On a previous numerical study we showed that using multiple-intermittent CSC spurts and laser pulses could permit, under certain conditions, the use of higher laser doses while providing sufficient epidermal protection. In this study we show some results of ongoing experimental to study the feasibility of implementing clinically such an approach.

1. INTRODUCTION

Cryogen spray cooling (CSC) has been used effectively during laser therapy to cool selectively the epidermis, while minimally affecting deeper targets such as port wine stain (PWS) birthmarks (150 to 500 μm deep) [1-2]. Clinical studies [2-4] have demonstrated that radiant exposures of 8-9 J/cm^2 are required to cause irreversible photocoagulation of PWS vessels in patients with higher epidermal melanin concentration (i.e., skin types V-VI). Unfortunately, the current approach to PWS laser therapy—consisting of a single cryogen spurt and a single laser pulse (SCS-SLP approach) does not provide sufficient epidermal protection for patients with darker skin types. Consequently, radiant exposures are still limited to avoid non-specific thermal injury.

Recent studies have sought to optimize cryogen spurt durations to maximize the temperature difference between the epidermis and PWS vessels [5,6] and others have focused on maximizing the cooling efficiency (η) by different means [7-12]. Besides these studies on CSC, other alternatives, which involve multiple laser pulses to the same treatment site, have also been investigated. Anvari et al. [13,14] proved the utility of applying intermittent cryogen spurts along with continuous laser irradiation to cause deeper tissue photocoagulation using a 1064 nm wavelength Nd:YAG laser. A more recent study by Verkruysse et al [15] introduced a mathematical model that supports the use of multiple laser pulses as a mean to target optically shielded blood vessels, which fail to respond to the current approach of a single laser pulse. We have recently developed [16] a four-layer computer model that integrates algorithms of heat diffusion, light distribution, and tissue damage, to investigate what is the minimum η required to obtain a safe and effective treatment for PWS patients with darker skin types. We have used this model to run simulations of both, the current approach of a single cryogen spurt followed by a single laser pulse (SCS-SLP), and a new approach consisting of multiple cryogen spurts applied intermittently with multiple laser pulses (MCS-MLP). Our results showed that patients with darker skin types (e.g., V-VI) are not suitable candidates for PWS treatment using SCS-SLP for a 585-595 nm pulsed-dye laser exposure, even for η = 100%. In contrast, numerical simulations of MCS-MLP provided adequate epidermal protection while inducing the desired PWS vessel damage for patients with skin types V-VI.

We have now taken a step forward and continue to study the feasibility of such an approach. For that purpose we have started to design a MCS-MLP experimental procedure that will allow us to test our model predictions.

At this stage, we have only focused on obtaining reliable temperature measurements for each of the absorbing layers (epidermis and PWS). In future work, we will aim at assessing the thermal damage that the predicted experimental conditions induce on human tissue. In this work, we describe the details of our experimental apparatus and present preliminary results carried out on skin phantoms.

2. MATERIALS AND METHODS

Finite Difference 4-layer Numerical Model

In our original numerical model [16], we modeled PWS human skin as an axi-symmetric, semi-infinite cylinder composed of four layers (Figure 1): an epidermal melanin layer, a dermis layer, a PWS layer, and a deeper dermis layer below the PWS.

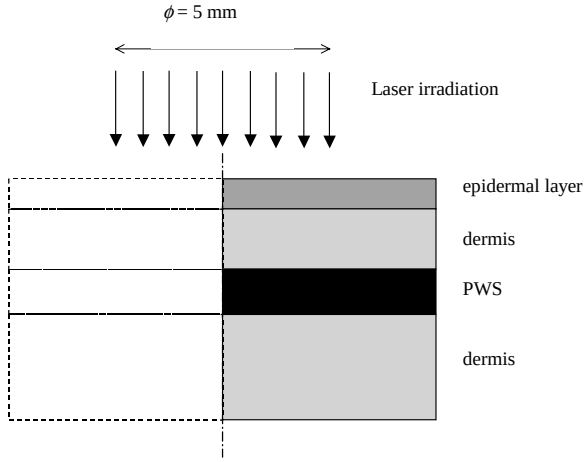

Figure 1: Four-layer model of PWS human skin. The shaded areas represent the discretized cross section, which consists of 15 mm in the radial direction and 1 mm in the axial direction discretized into 60 and 100 nodes, respectively.

A 2D forward-time, central space finite difference (FD) approximation to the heat diffusion equation was used to compute the spatial and temporal distribution of skin temperature during CSC and after laser exposure. Due to symmetry, only half of the irradiated skin cross section was used (15 mm wide by 1 mm thick) and it was discretized into 60 and 100 nodes, respectively. The skin layers thickness, and thermal (thermal conductivity k, density ρ, specific heat c, and thermal diffusivity α) and optical properties (absorption coefficient μ_a, scattering coefficient μ_s, anisotropy factor g, and index of diffraction n) used in our previous study [16] are listed in Table 1. The optical properties correspond to a 585 nm wavelength, and they are the same reported and used in previous studies [16-19]. It was assumed that both chromophores of interest, melanin and hemoglobin, had a homogeneous spatial distribution within the epidermis and PWS, respectively. The epidermal absorption coefficient of 80 cm^{-1} corresponds to a melanin volume fraction, v_{fm}, of 20% (skin types V-VI), assuming a melanosome absorption coefficient of 400 cm^{-1} at 585 nm [20]. The PWS layer absorption coefficient of 19.1 cm^{-1}, corresponds to a blood volume fraction, v_{fb}, of 10% [21].

Table 1: Thickness, and thermal and optical properties of layers used with the 4-layer FD model.

	Layer			
Properties	**Epidermis**	**Dermis**	**PWS**	**Dermis below PWS**
thickness [μm]	50	150	200	>>1,000
k [W/(m K)]	0.21	0.53	0.55	0.53
ρ [kg/m^3]	1,200	1,200	1,100	1,200
c [J/(kg K)]	3,600	3,800	3,600	3,800
α [m^2/s]	4.86×10^{-8}	1.16×10^{-7}	1.39×10^{-7}	1.16×10^{-7}
μ_a [cm^{-1}]	80	2.4	19.1	2.4

μ_s [cm^{-1}]	470	129	467	129
g	0.79	0.79	0.99	0.79
n	1.37	1.37	1.33	1.37

Polyacrylamide Gel Phantoms

For our present experiments, acrylamide gel phantoms were used to simulate multi-layered composite human skin with non-absorbing and absorbing layers. Phantoms were ~ 20% acrylamide gels made by adding 9.7 g of acrylamide and 0.3 g of bis-acrylamide (Sigma Chemical, St. Louis, MO) to 50 ml of deionized water. Direct Red 81 (Sigma Chemical, St. Louis, MO) was used to create optical absorption at 532 nm. The optical absorption of the dye was determined with a spectrophotometer (8452A Diode Array Spectrometer, Hewlett Packard, Waldbronn, FRG). Ammonium persulfate and tetra-methylethylenediamine (TEMED) (Sigma Chemical, ST. Louis, MO) were used to initiate polymerization of the solution into a gel.

Acrylamide solutions were injected between glass slides with plastic feeler gauge stock (McMaster-Carr, Los Angeles, CA) used as spacers. Thicknesses of the feeler gauge stock and gels were verified using a micrometer with 1μm resolution (Mitutoyo micrometer, McMaster-Carr, Los Angeles, CA). Layered gels were made to mimic epidermis, bloodless dermis, and PWS. More detailed information about the fabrication of these phantoms has been previously documented [22,23].

Laser

To the best of our knowledge, a 585-595 nm wavelength laser that can be pulsed at 50-60 Hz with fluences of ~ 1-4 J/cm^2, as used in our 2D-FD model is currently not available. Therefore, we have used a frequency-doubled 532 nm wavelength, Nd:YAG laser (Verapulse VPW, Lumenis, Inc. Santa Clara, CA), which has been modified to operate at a frequency of 16.8 Hz, pulse duration from 1 to 2 ms and a maximum pulse energy of 500 mJ. This laser wavelength is no longer considered a gold standard for PWS and other vascular lesion therapies because the melanin absorption at this wavelength is slightly higher and the hemoglobin absorption is slightly lower than 585 nm, but it is still used occasionally for this kind of treatment and is convenient for our planned experiments. Light was delivered to the sample via a 365μm diameter, 0.20NA optical fiber that was coupled to a zoom handpiece with a fixed working distance. This arrangement provided a spot size variable from 2–10 mm in diameter. For our experiments we used a 4 mm spot diameter, a 2 ms pulse duration and an average pulse energy of 140 mJ, which based on the other fixed parameters leads to an average fluence of 1.1 J/cm^2.

Cryogen Delivery

A commercial cryogen spray nozzle used for laser treatment of vascular lesions and hair removal (GentleLASE^{TM}, Candela, Wayland, MA), with an inner diameter of 0.5 mm was used to deliver short cryogen spurts. Liquid cryogen (tetrafluoroethane, R-134a, boiling temperature, T_b = –26^{o}C, at atmospheric pressure) was delivered through a standard high-pressure hose connecting the container to a control valve. The container is pressurized at the saturation pressure of this cryogen (6.7 bar at 25^{o}C). Spurt durations—defined by the time the valve remains open, were electronically controlled. For all experiments, the nozzle tip was position at approximately 35 mm from the sprayed surface.

Layer Temperature Measurements

To measure the temperature profiles during and after laser exposure, we have used a Raytheon IR camera (Model Galileo, Dallas, TX) and used pulsed photothermal radiometry (PPTR) to reconstruct the temperature profiles. The frame rate was fixed at 1,000 fps and the integration time τ = 0.9 ms using a 4.5-5 μm detection bandwidth. Each PPTR signal was used as input into an iterative conjugate gradient based inversion algorithm developed for PWS depth profiling [24]. The algorithm is designed to compute the initial 1-D space resolved temperature profile in an object immediately following the incident laser pulse. The criterion for optimal iteration number selection is analysis of the L-curve, which is a plot of the log of the squared norm of the regularized solution versus that of the regularized residual [25]. Reconstructed profiles consisted of either 13

(for the epidermis-dermis phantom geometry) or 64 (for the dermis-PWS phantom geometry) points spaced evenly at an interval of ~16 μm.

Due to the difficulty in interpreting PPTR signals from deeply embedded layers, we separated the experiment into two sets. The first set involved a dermal and PWS layers (dermis-PWS configuration) and the second set involved an epidermal and dermal layer (epidermis-dermis configuration). Laser irradiation and CSC were applied to these sets with the intention of superimposing the reconstruction results as an interpretation of a three-layer structure made up of epidermis, dermis, and PWS. The PWS layers were 190 μm thick with and absorption coefficient of 60 cm^{-1}. They rested beneath a clear layer of 1 mm thickness. The epidermis layers were 70 μm thick and had two absorption coefficients, 30 and 100 cm^{1}, representing light and dark skin, respectively. The epidermal layer rested on a clear layer with 150 μm thickness, representing bloodless dermis. For each experiment, the 2-layer configuration was placed on an acrylic slab mounted on an optical post and fixed with rubber bands. The slab had a 6 mm hole bored out of the center for PPTR imaging.

Figure 2 shows a schematic of the arrangement of the PA gel phantoms, the laser, the cryogen nozzle, and the PPTR camera.

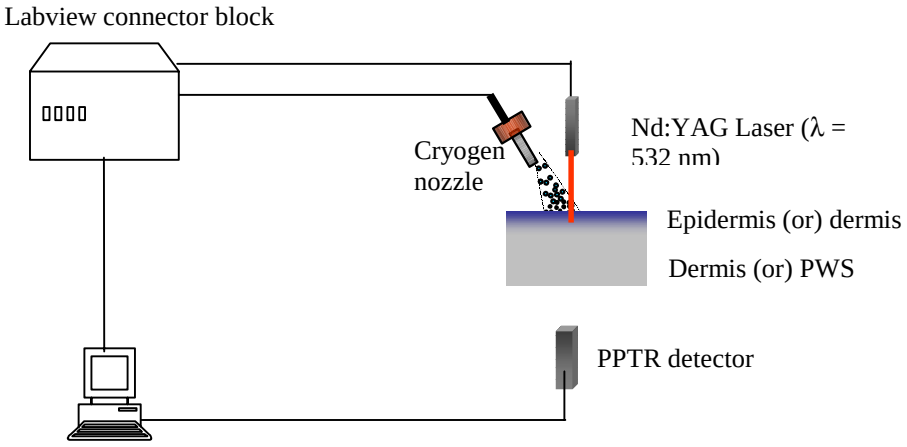

Figure 2. Schematic of MCS-MLP experimental procedure.

Synchronization and Data Acquisition

Multiple cryogen spurts and laser pulses were electronically controlled using a custom-made program in LabVIEW™ (v.6i, National Instruments, Austin, TX) software run on a PC pentium computer. Data input and control outputs were handled by a connector block (Model BNC-2110, National Instruments) wired to a data acquisition board (Model PCI-6110E, National Instruments). The same time diagram used for our previous numerical model simulations was implemented for these experiments, which is shown in Figure 3.

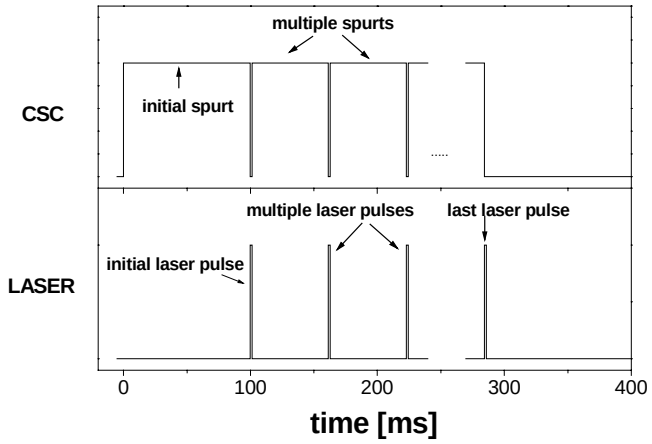

Figure 3. Time diagram of the MCS-MLP experimental procedure.

The whole sequence consists of an initial 100 ms spurt, followed by *n* subsequent laser pulses intermittently applied with 60 ms cryogen spurts. This time sequence corresponds to a repetition rate of 16.6 Hz. For our experiments, we used n = 1, 2, 3, 5,10, and 20. It was noticed during the experiments that the fluence of laser pulses was increasing systematically during the first 8-10 pulses, after which the energy per pulse stabilized. Therefore, a mechanical shutter (Uniblitz, Model D122, Rochester, NY) was introduced between the laser and the layer's upper surface to block the first 10 pulses.

Finite Difference 2-Layer Model

A 1D-FD heat diffusion model was developed to facilitate the generation of theoretical temperature profiles that resembled our experimental conditions. This model incorporates the instantaneous laser pulse profile to compute the heat generation for each pulse, calculates the temperature profiles as a function of time and the instantaneous radiometric temperature raise $\Delta S(t)$, at the surface facing the IR camera, which is given by:

$$\Delta S(t) = \mu_{ir} \int_0^{z_f} \Delta T(z,t)\, e^{-\mu_{ir} z}\, dz, \tag{1}$$

where μ_{ir} is the infrared attenuation coefficient (265 cm^{-1}) [26], ΔT is the local and temporal variation of tissue temperature and z_f is the total layer depth measured from the surface facing the IR camera.

3. RESULTS AND DISCUSSION

Previous Numerical Results

Figure 4 shows show an example of the potential of the MCS-MLP approach. It shows the temperature profiles as a function of depth at the end of each laser pulse as computed by the 4-layer FD model, for a 585 nm wavelength laser applied to a patient with relatively dark skin (melanin volume fraction, v_f of 20%, which roughly corresponds to a skin type V or VI). The target is composed of a PWS vessel cluster 200 μm deep and 200 μm thick. It was shown before [16], that the skin thermal resistance may prevent the successful implementation of the current SCS-SLP approach for patients with this skin types, even for η = 100%. In contrast, a total of 14 cryogen spurts intermittently applied with a lower laser fluence (4 J/cm^2) and a more realistic cooling efficiency (η = 75%), were adequate to induce a significant thermal damage to the PWS (Ω_{PWS}) while keeping the epidermal thermal damage (Ω_E) below a pre-specified threshold for the same skin type. It was assumed that Ω_E is excessive if it exceeded a value of 1, which corresponds to a 63% decrease from the original total undamaged tissue constituents.

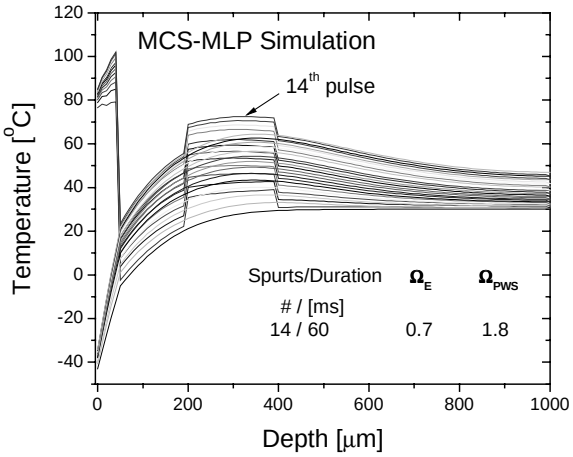

Figure 4. MCS-MLP approach for a patient with skin type V or VI. Each curve illustrates, respectively, the skin temperature at the end of the 14 laser pulses used for this simulation.

It is important to point out that the purpose of a MCS-MLP approach is to maximize PWS thermal damage while minimizing epidermal injury. This can only be successful if two conditions are met: (1) the energy generated within the PWS vessels by each laser pulse is greater than that lost by diffusion between two consecutive pulses; and (2) cryogen spurts applied intermittently with laser pulses maintain the epidermal temperature below the threshold for thermal damage.

Dermis-PWS Configuration

Figure 5 shows the radiometric temperature, $S(t)$, computed by the 2-layer model for the dermis-PWS configuration for $n = 15$. The solid and dashed curves represent the cases where no CSC and CSC were applied, respectively. $t = 0$ represents the onset of the first laser pulse and the onset of the first cryogen spurt for the cases no CSC and CSC, respectively.

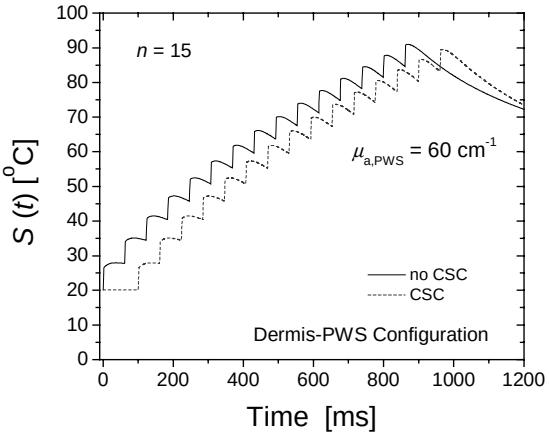

Figure 5. Radiometric temperature variation computed by the 2-layer model for the dermis-PWS configuration. The solid and dashed lined represent the case where no CSC and CSC were used, respectively.

It becomes evident from this Figure that under ideal experimental conditions, the effect of CSC on $S(t)$ induces basically a time-shift equal to the duration of the first spurt (100 ms). This situation is actually advantageous because it is expected that the light transmittance will decrease when CSC is applied [27]. In fact, according to a recent work [27], the light transmittance decrease can be as large as 15% immediately after a 100 ms spurt. Therefore, carrying out the experiments without CSC for this configuration will not introduce a significant variation in the measured temperature, while light transmittance issues will be avoided.

The advantage of not having to use CSC is quite evident when we look at the PPTR reconstructions carried out for this configuration under no CSC. Figure 6a shows the 2-layer model curve (solid), the temperature reconstruction based on this curve (dashed) and the experimental temperature reconstruction (dotted), right after the termination of 5 laser pulses. The oscillations seen for the reconstructed curves may be due to instabilities of the PPTR reconstruction algorithm but, by and large, the magnitude of the temperature rise seems to be accurately measured. In contrast, when CSC is used (Figure 6b), the temperature rise is affected by more than 6°C out of a 12°C rise predicted by the 2-layer model, even after only 1 pulse.

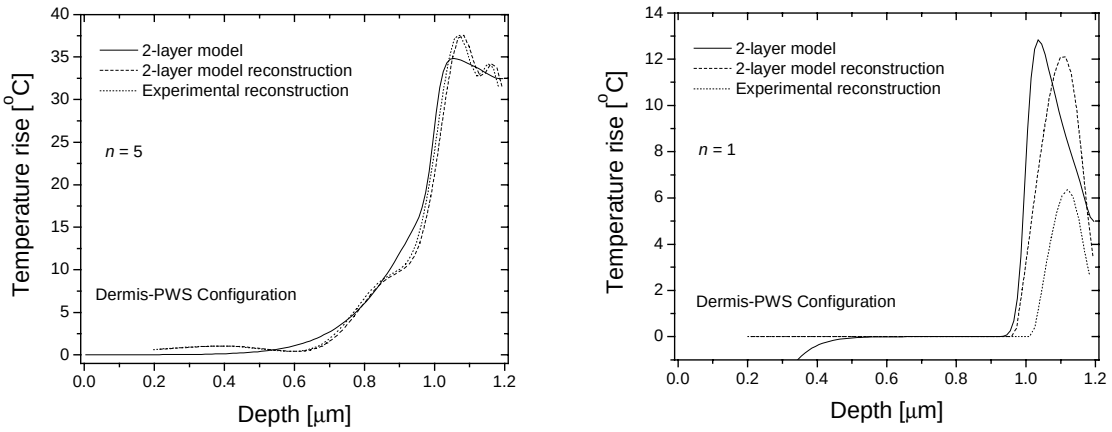

Figure 6. (a) Comparison of Radiometric temperature reconstructions between the 2-layer model and experimental conditions for the Dermis-PWS configuration without the use of CSC, n = 5. **(b)** With CSC, n = 1.

Figure 7 shows S(t) during numerical and experimental MCS-MLP procedures where n = 13-15. The solid curve represents the radiometric temperature that would be theoretically measured if we removed the bottom dermis layer from the 4-layer model (PWS skin model), *i.e.*, the radiometric at the bottom edge of the 200 μm thick, 200 μm deep PWS layer. The dashed curve represents the $S(t)$ predicted for the actual, ideal experimental conditions when using CSC (same curve shown in Fig. 5). The dotted line represents the measured $S(t)$. The variation of $S(t)$ under the 2-layer model or ideal experimental conditions (dashed line) is similar to that computed by the 4-layer model (solid line) during the first pulses. Toward the end of the sequence of pulses, however, the 2-layer model leads to a somewhat higher temperature. This is due to the adiabatic boundary at the bottom edge of the PWS layer, which induces an excessive heat accumulation, as opposed to the 4-layermodel where there is essentially a semi-infinite medium for the heat to diffuse (*i.e.*, thick dermis layer below the PWS layer). The experimental curve (dotted) shows somewhat lower $S(t)$. For the 4-layer model, the fluence at the upper edge of the PWS layer is estimated to be about 1.5 J/cm^2, *i.e.*, about 1.4 times higher the one used for the experiments. Additionally, the transmittance through the cryogen layer is expected to be reduced by 15% [27], as mentioned above. Therefore, if we divide the 4-layer computed radiometric temperature by a constant factor of 1.4 to account for the reduced fluence, and by 1.15 to account for the reduced transmittance, we obtain the curve shown also in Figure 6 (dash-dot), which shows a much better fit with the measured data. This is a crude approximation considering the transmittance decrease is also a dynamic event, which likely increases rapidly at the beginning of the spurt and reaches a plateau towards spurt termination, but it is obviously a reasonable first-degree approximation. The over-prediction of $S(t)$ by the 2-layer model indicates us that, for future experiments, we should place a thin clear layer at the back of the PWS layer or, alternatively, provide some cooling mechanism, *e.g.*, air cooling, that does not interfere with the IR camera view and helps remove excessive PWS layer heating.

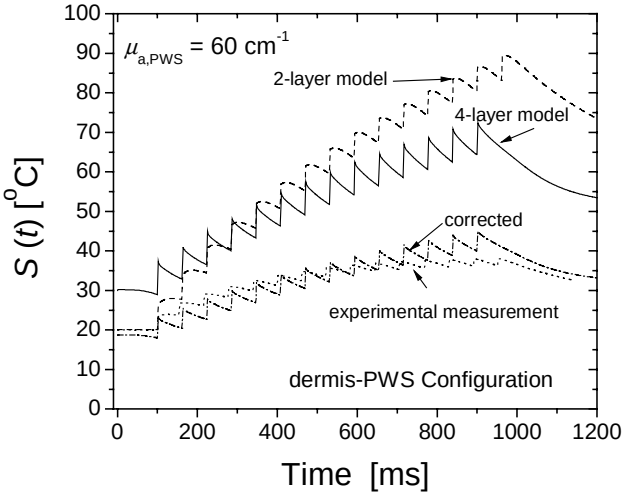

Figure 7. Radiometric temperatures for the dermis-PWS configuration. 4-layer model (solid), 2-layer model (dashed), experimental (dotted), and corrected (dash-dot).

Epidermis-Dermis Configuration

Figure 8 shows radiometric temperatures, $S(t)$, computed by the 2-layer model for the epidermis-dermis configuration. The solid and dashed curves represent the cases where no CSC and CSC were applied, respectively. The results for the two epidermal layer absorption coefficients, μ_a = 30 and 100 cm^{-1}, are presented in this figure. It becomes evident that under ideal experimental conditions, the effect of CSC on $S(t)$ is very large, and even for the case where μ_a = 100 cm^{-1}, the expected radiometric signal would be barely above 0°C. As for the case presented in Figure 5, it is also to be expected that the light transmittance is reduced under real experimental conditions after or between consecutive cryogen spurts, which would in turn reduce $S(t)$ even further. In fact, preliminary experiments using CSC showed essentially continuous cooling during a MCS-MLP procedure. This suggests that in order to resemble the epidermal heating seen on the 4-layer model approximation (Fig. 4), it may be necessary to increase the absorption coefficient of the epidermal layer and/or reduce η, or even eliminate completely CSC.

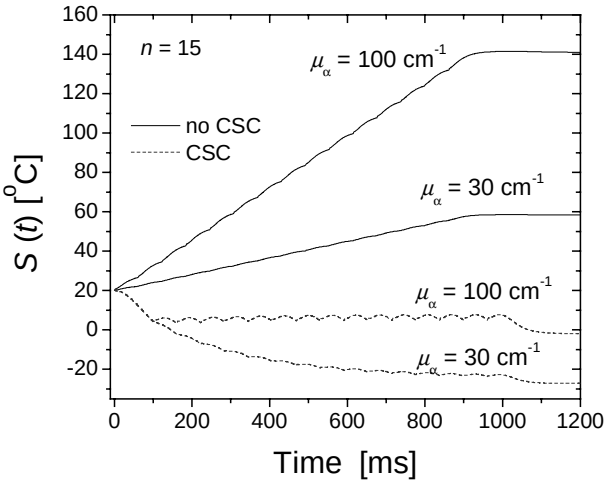

Figure 8. Radiometric temperature variation computed by the 2-layer model for the epidermis-dermis configuration. The solid and dashed lines represent the cases where no CSC and CSC was used, respectively, and two curves are shown for each case corresponding to μ_a = 30 and 100 cm^{-1}.

Figure 9 shows a comparison between the predicted and measured $S(t)$ for the epidermis-dermis configuration with μ_a = 30 cm^{-1}. The solid line represents the $S(t)$ that would result if the PWS and bottom dermis layers were removed from the 4-layer model (PWS skin model), *i.e.*, the radiometric temperature at the upper edge of the

200 μm thick, 200 μm deep PWS layer. The dashed curve represents the $S(t)$ predicted for the actual, ideal experimental conditions without using CSC (same curve shown in Fig. 8). The dotted line represents experimental measurement of $S(t)$ when no CSC is applied. Note that the 2-layer model prediction and the experimental curves are almost identical. Incidentally, both of these curves represent quite closely the maximum $S(t)$ computed by the 4-layer model. However, since no CSC was applied, the temperature oscillations are not as noticeable. A possible solution to obtain a better match for the temperature variation could be achieved by increasing μ_a and adjusting (reducing) η, to overcome excessive heating. Both of these solutions are simple to implement and will be considered for future experiments.

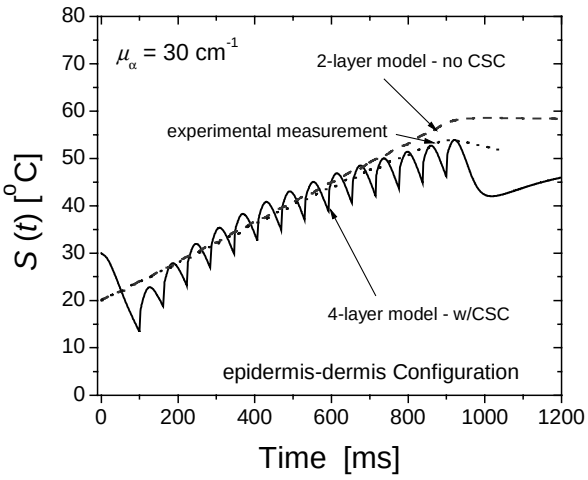

Figure 9. Radiometric temperatures for the epidermis-dermis configuration. 4-layer model (solid), 2-layer model without CSC (dashed), experimental without CSC (dotted) n = 10.

4. CONCLUSIONS

We have assembled a complete experimental procedure consisting of polyacrylamide gel tissue phantoms, a modified 532 nm Nd:YAG pulsed laser, and PPTR technique to measure the temperature increase within the tissue. This experimental procedure provides a flexible configuration to perform experiments under a large variety of conditions.

In our numerical simulations, the radiometric temperature estimate for the dermis-PWS configuration suggested that the effect of CSC at ~ 200 μm would not have a large impact on the PWS temperature variation. However, PPTR reconstructions of the experimental temperature profiles suggest that light scattering taking place during CSC [27] could affect significantly the temperature raise within the PWS, even after only 1 pulse. As a first-degree approximation, this situation was corrected by introducing a correction factor into the 4-layer model, which accounts for the decrease in light transmittance and the lower fluence used in our experiments.

The 2-layer simulations for the epidermal-dermal configuration showed that experiments with CSC would lead to very low radiometric temperatures, even in the absence of transmittance effects, which would decrease the energy generated within the epidermal layer even further. In contrast, both the experiment simulations (2-layer model) and the actual experimental data for the 30 cm^{-1} case without CSC, follow the overall trend of the temperature curve predicted by the 4-layer model, although not with the same amplitude. A possible solution to obtain more comparable temperature profiles could be achieved by increasing μ_a and adjusting the cooling efficiency (η) to overcome excessive heating. Both of these solutions are simple to take and will be considered for future experiments.

Future studies will aim at superimposing these temperature measurements and interpret the results of a 4-layer structure made up of epidermis, dermis, PWS and dermis, as in the original numerical model. We will also look into the epidermal thermal damage induced to artificial skin models (RAFT) to determine whether or not a MCS-MLP procedure could be viable for clinical implementation.

ACKNOWLEDGEMENTS

This work was supported by a research grant from the Institute of Arthritis and Musculoskeletal and Skin Diseases at the National Institutes of Health (GM62177 to JSN and HD42057 to GA). Institutional support from the Office of Naval Research, Department of Energy, and the Beckman Laser Institute and Medical Clinic Endowment is also acknowledged.

REFERENCES

[1] Nelson JS, Milner TE, Anvari B, Tanenbaum BS, Kimel S, Svaasand LO, and Jacques SL. Dynamic epidermal cooling during pulsed laser treatment of port-wine stain. Arch Dermatol 1995;131:695-700.

[2] Chang CJ and Nelson JS. Cryogen spray cooling and higher fluence pulsed dye laser treatment improve port wine stain clearance while minimizing epidermal damage. Dermatol Surg 1999; 25:766-771.

[3] Morelli JG, Weston WL, Huff JC, and Yohn JJ. Initial lesion size as a predictive factor in determining the response of port-wine stains in children treated with the pulsed dye laser. Arch Pediatr Adolesc Med 1995; 149:1142-1144.

[4] van der Horst CMAM, Koster PHL, deBorgie CAJM, Bossuyt PMM, and van Gemert MJC. Effect of timing of treatment of port-wine stains with the flash-lamp-pumped pulsed dye laser. N Engl J Med 1998; 338:1028-1033.

[5] Verkruysse W, Majaron B, Tanenbaum BS, and Nelson JS. Optimal cryogen spray cooling parameters for pulsed laser treatment of port wine stains. Lasers Surg Med 2000; 27:165-170.

[6] Tunnell JW, Nelson JS, Torres JH, and Anvari B. Epidermal protection with cryogen spray cooling during high fluence pulsed dye laser irradiation: an ex vivo study. Lasers Surg Med 2000; 27:373-383.

[7] Verkruysse W, Majaron B, Aguilar G, Svaasand LO, and Nelson JS. Dynamics of cryogen deposition relative to heat extraction rate during cryogen spray cooling. Proc SPIE 2000; 3907: 37-48.

[8] Aguilar G, Verkruysse W, Majaron B, Svaasand LO, Lavernia EJ, and Nelson JS. Measurement of heat flux and heat transfer coefficient during continuous cryogen spray cooling for laser dermatologic surgery. IEEE J Sel Top Quantum 2001; 7:1013-1021.

[9] Anvari B, Ver Steeg BJ, Milner TE, Tanenbaum BS, Klein TJ, Gerstner E, Kimel S, and Nelson JS. Cryogen spray cooling of human skin: effects of ambient humidity level, spraying distance, and cryogen boiling point. Proc SPIE 1997; 3192:106-110.

[10] Aguilar G, Majaron B, Pope K, Svaasand LO, Lavernia EJ, and Nelson JS. Influence of nozzle-to-skin distance in cryogen spray cooling for dermatologic laser surgery. Lasers Surg Med 2001; 28:113-120.

[11] Majaron B, Aguilar G, Basinger B, Randeberg LL, Svaasand LO, Lavernia EJ, and Nelson JS. Sequential cryogen spraying for heat flux control at the skin surface. Proc SPIE 2001;4244:74-81.

[12] Torres JH, Tunnell JW, Pikkula BS, and Anvari B. Cryogen spray cooling for dermatological laser therapy. Dynamics of cryogen deposition and effect of simultaneous airflow application. Lasers Surg Med 2001; 28:477-486.

[13] Anvari B, Tanenbaum BS, Milner TE, Tang K, Liaw LH, Kalafus K, Kimel S, and Nelson JS, Spatially selective photocoagulation of biological tissues - feasibility study utilizing cryogen spray cooling. Appl Optics 1996; 35: 3314-3320.

[14] Anvari B, Tanenbaum BS, Hoffman W, Said S, Milner TE, Liaw LH, and Nelson JS, Nd:YAG laser irradiation in conjunction with cryogen spray cooling induces deep and spatially selective photocoagulation in animal models. Phys Med Biol 1997; 42: 265-82.

[15] Verkruysse W, van Gemert MJC, Smithies DJ, and Nelson JS, Modelling multiple laser pulses for port wine stain treatment, Phys. Med. Biol. 2000; 45:N197-N203.

[16] Aguilar G, Diaz SH, Lavernia EJ, and Nelson JS, Cryogen spray cooling efficiency: Improvement of port wine stain laser therapy through multiple-intermittent cryogen spurts and laser pulses, Lasers Surg Med, 2002; 31:27-35.

[17] Duck FA. Thermal properties of tissue. Physical properties of tissue. London: Academic press; 1990.

[18] van Gemert MJC, Welch AJ, Pickering JW, and Tan OT. Laser treatment of port wine stains. In: Welch AJ, van Gemert MJC, editors. Optical-thermal response of laser irradiated tissue. New York: Plenum Press; 1995.
[19] Pfefer TJ, Smithies DJ, Milner TE, van Gemert MJC, Nelson JS, and Welch AJ. Bioheat transfer analysis of cryogen spray cooling during laser treatment of port wine stains. Lasers Surg Med 2000; 26: 145-157.
[20] Jacques SL, Glickman RD, and Schwartz JA. Internal absorption coefficient and threshold for pulsed laser disruption of melanosomes isolated from retinal pigment epithelium. Proc SPIE 1996; 2681:468-477.
[21] Verkruysse W, Pickering JW, Beek JF, Keijzer M, and van Gemert MJC. Modeling the effect of wavelength on the pulsed dye laser treatment of port wine stains. Appl Opt 1993; 32: 393-398.
[22] Viator JA, Jacques SL, and Prahl SA. Depth profiling of absorbing soft materials using photoacoustic methods. IEEE J Sel Top Quant 1999; 5: 989-996.
[23] Bini MG, Ignesti A, Millanta L, Olmi R, Rubino N, and Vanni R. The polyacrylamide as a phantom material for electromagnetic hyperthermia studies. IEEE Trans Biomed Eng 1984; 31:317-322.
[24] Milner TE, Goodman DM, Tanenbaum BS, and Nelson JS. Depth profiling of laser-heated chromophores in biological tissues by pulsed photothermal radiometry. J Opt Soc Am A 1995; 12**:**1479-1488.
[25] Johnston PR and Gulrajani RM. Selecting the corner in the L-curve approach to Tikhonov regularization. IEEE T Bio-Med Eng 2000; 47**:**1293-1296.
[26] Majaron B, Verkruysse W, Tanenbaum BS, Milner TE, Telenkov SA, Goodman DM, and Nelson JS. Combining two excitation wavelengths for pulsed photothermal profiling of hypervascular lesions in human skin. Phys Med Biol 2000; 45**:**1913-1922.
[27] Edris A, Choi B, Aguilar G, and Nelson JS. Measurements of Laser Light Attenuation by Cryogen Film during Dynamic Epidermal Cooling, Lasers Surg Med 2003; 32, N2—in press.